

AI-Driven Stabilization in Power Grids through Controlling Line Admittances

Sangjoon Park,¹ Hoyun Choi,² Yongsun Lee,³ Seungchan Jo,⁴ Jürgen Kurths,⁵ and B. Kahng¹

¹*CCSS, KI for Grid Modernization, Korea Institute of Energy Technology, Naju, Jeonnam 58330, Korea*

²*School of Computational Sciences, Korea Institute for Advanced Study, Seoul, 02455, Korea*

³*CTP and Department of Physics and Astronomy, Seoul National University, Seoul 08826, Korea*

⁴*Department of Electrical and Computer Engineering, Seoul National University, Seoul 08826, Korea*

⁵*Potsdam Institute for Climate Impact Research, Telegrafenberberg, D-14415, Potsdam, Germany*

(Dated: January 6, 2026)

The global transition from traditional power plants to renewable energy sources introduces new challenges in grid stability, primarily because inverter-based technologies provide insufficient inertia. To address this, we introduce an artificial intelligence algorithm that autonomously stabilizes power grids by adaptively tuning admittance regulators in response to disturbances. This Adaptive Admittance Controller (AAC) algorithm not only stabilizes the system in real time but also identifies the best regulator locations, thereby unifying grid planning and real time control within a single framework. When tested on a real UK power grid, the AAC markedly reduces frequency deviations and rapidly restores nominal operation. In addition, the algorithm isolates a small number of key regulators and intervenes only on these, lowering both system complexity and cost. The AAC algorithm further reduces the nonlinearity effect, quickly stabilizing the frequency and power flow. This intelligent control scheme enables power grids to reliably return to stable operating conditions under a broad spectrum of fault scenarios. The proposed framework can also be used to mitigate cascading failures by adaptively controlling critical links in a variety of networked infrastructures, such as cascades of traffic congestion on road networks or fuse failures in energy-saving systems.

I. INTRODUCTION

Electrical power grids underpin modern society, enabling almost every aspect of daily life—from hospitals and data centers to residential and industrial operations [1, 2]. The worldwide move toward carbon-neutral energy systems represents one of the most ambitious infrastructure overhauls in human history. Yet this transformation also brings significant vulnerabilities: as renewable resources replace traditional generators, power systems lose the rotational inertia that has historically damped disturbances, endangering the stability that billions of people rely on [3–6].

The replacement of synchronous generators with inverter-based resources diminishes overall system inertia, making the grid more vulnerable to frequency disturbances. At the same time, the intrinsic variability of renewable sources introduces a level of operational complexity not previously encountered [7–9]. These challenges become even more pronounced during transmission line outages, where the loss of a single line can set off cascading instabilities throughout interconnected networks.

Recent large-scale blackouts illustrate the severe impact of grid instability. The 2019 UK blackout [10] and the 2021 Texas power crisis [11, 12] were both triggered by transmission line outages caused by extreme weather, putting millions of people at risk and resulting in economic losses of billions of dollars. These incidents underscore the urgent demand for new stability management approaches that can function reliably in grids with a high share of renewable generation [13–15].

Frequency is a primary real-time metric for assessing the balance between power supply and demand [16, 17]. Under normal conditions, it is carefully maintained within

tight bounds; nonetheless, transmission line faults can trigger abrupt deviations that endanger both global and dynamic stability [18]. Rapid suppression of these frequency excursions is crucial to prevent cascading failures, which may lead to large-scale blackouts and severe economic as well as social consequences [19–21]. The evolution of system frequency is typically described by the swing equation [22, 23].

Traditionally, stability has been improved by modifying the infrastructure, either by constructing additional transmission lines or upgrading existing ones [24, 25]. Yet, these approaches are increasingly hindered by public opposition, substantial costs, protracted permitting procedures, and environmental concerns [26, 27]. In recent years, numerous works have investigated boosting grid stability through flexible alternating current transmission system (FACTS) devices, such as thyristor-controlled series capacitors (TCSCs) [28–30], which regulate the admittance of transmission lines. Their overall benefit, however, is constrained by two tightly linked issues: determining where to install them (a planning task) and how to tune their admittances in operation (an operational task). The enormous combinatorial space of possible regulator deployments and settings makes conventional optimization techniques computationally demanding, and poorly chosen configurations may even worsen stability.

These challenges align well with reinforcement learning (RL), which is adept at handling high-dimensional optimization problems in dynamical systems. RL has achieved notable success in a wide range of autonomous systems by enabling consistent and adaptive control strategies [31–35]. Within power grid applications, RL-based methods have shown promise for tasks such as power dispatch—i.e., regulating power supply levels [36]—and for admittance

control of individual transmission lines [37, 38].

Such studies, however, treat planning and operation as distinct stages: they first determine regulator placements on inter-area tie-lines and only then design control schemes for those predetermined sites. Although this decoupled methodology is computationally tractable, it is fundamentally suboptimal. Once regulator locations are fixed, it is impossible to realize truly optimal control for faults arising at different points in the system.

To this end, we propose an Adaptive Admittance Controller (AAC) algorithm that autonomously stabilizes the power grid by adaptively tuning the admittance of transmission lines in response to line outages. By integrating both planning and real-time operation, the RL-based algorithm demonstrates two key capabilities: (i) performs intelligent, selective intervention by strongly mitigating high-risk contingencies while avoiding superfluous actions during minor disturbances; (ii) determines the minimum necessary subset of transmission lines on which to install regulators to achieve near-optimal control, thereby substantially reducing deployment costs. Evaluating more than 105 fault scenarios in a simplified UK national grid model [16], our approach provides a computationally efficient and economically viable solution, supporting the secure operation of future power systems with high penetrations of renewable energy sources.

II. FREQUENCY STABILIZATION AND ESSENTIAL PLACEMENTS

We employ two power grids: the UK power grid with a reduced number of buses and lines [16] and a synthetic so-called SHK grid [39]. In the main text, we present results for the UK power grid, while those for SHK are in

the Supplementary Information (SI).

A. Optimal reduction of frequency fluctuations

The frequency dynamics of the power grid is described by the swing equation [22, 23]:

$$m_i \ddot{\theta}_i + \gamma_i \dot{\theta}_i = P_i + \sum_{j \neq i} K_{ij} \sin(\theta_j - \theta_i), \quad (1)$$

where m_i represents the inertia of the turbine in the bus $i = \{1, \dots, N\}$. Note that m_i in the UK grid is highly heterogeneous due to the mixture of various generators. θ_i and $\dot{\theta}_i$ are the phase and angular velocity of the oscillator in the bus i ; γ_i is the damping coefficient; and P_i is the power ($P_i > 0$ for generators and $P_i < 0$ for consumers), which must satisfy the balance condition $\sum_i P_i = 0$. The coupling strength is composed of $K_{ij} = V_i V_j Y_{ij}$, where V_i and V_j are the voltages of the buses i and j , which are set to 1 under the assumption that the system is limited to the high voltage AC level, and Y_{ij} is the admittance of the transmission line between the buses i and j . $Y_{ij} = 0$ if buses i and j are not connected. $N = 54$ and the total number of lines L in the UK grid is 114. In the stable state, the system maintains a steady state with $\dot{\theta}_i = 0$.

To simulate a single transmission line fault between bus u and v , we set $Y_{uv} = K_{uv} = 0$. Due to the heterogeneity of buses, the complex grid topology, and their nonlinear dynamics [Eq. (1)], each line fault results in highly disparate responses across the entire system. Therefore, we consider all single-line failure scenarios that do not disconnect the grid, and specifically, 105 lines for the UK grid.

The frequency fluctuation triggered by a fault in line $\ell = (u, v)$ is measured as $\Xi^{(\ell)}$ [36]:

$$\Xi^{(\ell)} = \frac{1}{T} \int_0^T dt \left[\frac{1}{\sum_i m_i} \sum_i m_i \dot{\theta}_i^2(t) - \left(\frac{1}{\sum_i m_i} \sum_i m_i \dot{\theta}_i(t) \right)^2 \right], \quad (2)$$

where T is the measurement time, which is set to 10 seconds. $\Xi^{(\ell)}$ can be understood as inertia-weighted frequency fluctuations as a consequence of the line fault ℓ . Fig. 1(a) shows $\Xi^{(\ell)}$ for each line fault on a logarithmic scale. The scale of $\Xi^{(\ell)}$ varies widely among failures: the largest value is about 10^7 times larger than the smallest. This wide range of heterogeneity highlights a key challenge in distinguishing between failures that require intervention from those where intervention may not be necessary or even harmful.

The AAC algorithm addresses this challenge through a selective intervention. It consists of a graph neural network (GNN) designed to output an admittance adjustment for all transmission lines based on the power grid state and

line failure. For the detailed implementation of AAC algorithm, see Sec. V. Fig. 1(b) compares $\Xi^{(\ell)}$ for each line failure, with (orange) and without (green) adjustment applied via the AAC algorithm. In the plot, the x -axis represents all single-line faults in the UK power grid, ordered by the uncontrolled values of $\Xi^{(\ell)}$, such that higher impact failures appear on the left. In the range where $\Xi^{(\ell)}$ is large, the AAC algorithm substantially reduces its value, whereas in low-impact regions, the values are nearly identical. This indicates that the AAC algorithm effectively suppresses frequency fluctuations in severe failures, while avoiding non-necessary intervention in minor failures. Although one low-risk scenario shows a slight increase in $\Xi^{(\ell)}$, highlighting the importance of deciding

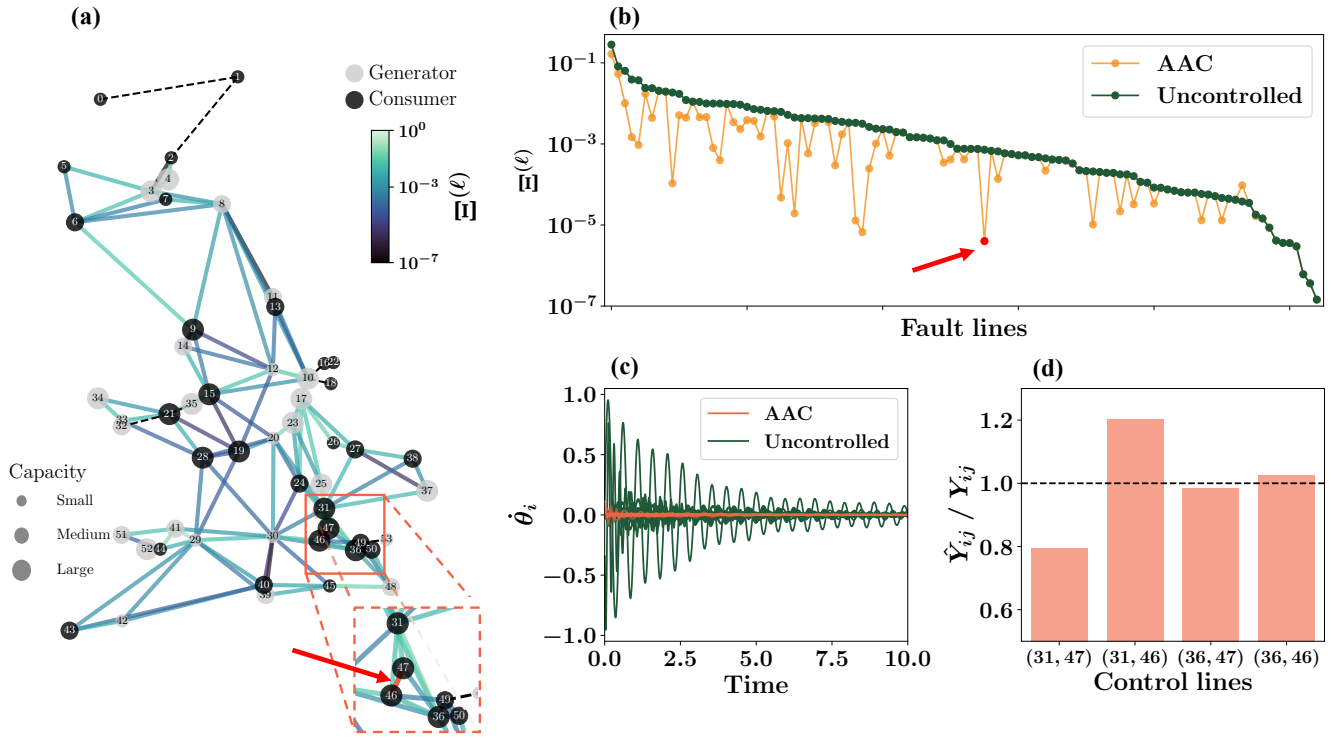


FIG. 1. Performance of the AAC algorithm under single-line failures in the UK power grid. (a) The color on each line (u, v) indicates $\Xi^{(\ell)}$ in Eq. (2). Node size indicates the absolute value of the power supply $|P_i|$ while generators are marked in gray and consumers in black. Dashed black lines indicate the lines excluded from our consideration as they disconnect the grid. (b) Comparison of the performance of the AAC algorithm for each fault case: controlled fluctuations (orange) vs. the uncontrolled case (green). In (a) and (b), the red arrows indicate the line between buses 46 and 47, selected as a well-behaved line for our studies, and exhibit the responses in (c) and (d). (c) Time evolution of the angular velocities $\dot{\theta}_i$, showing that the AAC algorithm (orange) rapidly suppresses the system's fluctuations. (d) The ratio of the adjusted admittance \hat{Y}_{ij} by the AAC algorithm to the original admittance Y_{ij} .

whether to intervene, its magnitude remains far below high-risk levels and does not pose a threat to overall stability. On average, it decreases $\Xi^{(\ell)}$ by approximately 53%.

Figs. 1(c) and (d) illustrate the cases marked in a red-filled circle in Fig. 1(b), which corresponds to the line fault between buses 46 and 47, marked with an arrow in Fig. 1(a). Fig. 1(c) shows that after applying the AAC algorithm, the oscillations are drastically suppressed in the amplitudes of the angular velocities compared to those in the uncontrolled case. Fig. 1(d) presents the adjustments in the selected line admittance. It reveals that stabilization requires control of only a few lines and often involves both increasing and decreasing admittance.

In summary, the AAC algorithm efficiently reduces frequency fluctuations, particularly for lines with high volatility. In contrast, it avoids superfluous intervention for lines with low volatility, where its effect is negligible. This targeted and resilient approach is crucial for practical applications, as it enhances system stability and reduces unnecessary control actions and resource utilization.

B. Optimal placement of regulators

Although the AAC algorithm is trained in an environment where it can control the admittance of all non-failed lines, in practice it is observed to control only a few lines. Using its behavior, we can reduce the number of admittance regulators in advance, enabling cost-effective operation.

Previous research in this regard used the power transfer distribution factor (PTDF) approach [40], which focuses on how the current flow in each line responds to a change in the power of a specific bus. This approach does not account for the case where the admittance of a particular line is changed. To bridge this gap, we present three ranking metrics for the line (i, j) grounded on the average behavior of the AAC algorithm in various fault scenarios.

$S^{(1)}$: The number of scenarios where the AAC algorithm controls line (i, j) .

$S^{(2)}$: The ratio of admittance changed by the AAC algorithm to the original value, \hat{Y}_{ij}/Y_{ij} .

$S^{(3)}$: The difference in admittance changed by the AAC

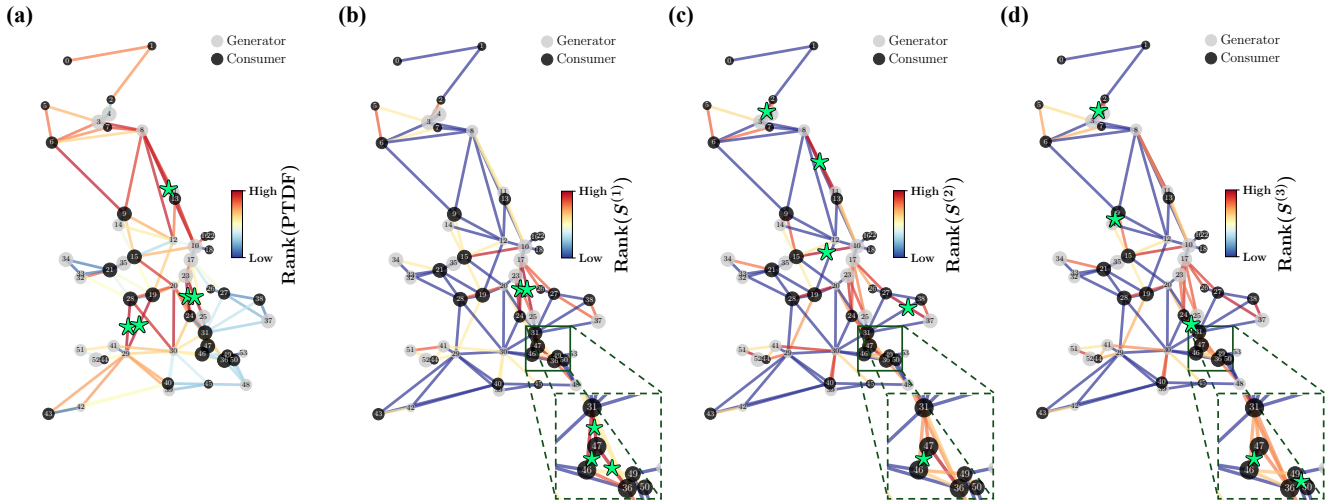


FIG. 2. Rankings of transmission lines for each metric, (a) the PTDF; (b) $S^{(1)}$; (c) $S^{(2)}$; and (d) $S^{(3)}$. The top five-ranked lines for each metric are marked with green stars. The significant differences between the top five-ranked lines selected by the traditional method (a) and by the AAC algorithm (b-d) demonstrate the importance of using control-aware criteria to identify critical regulator locations.

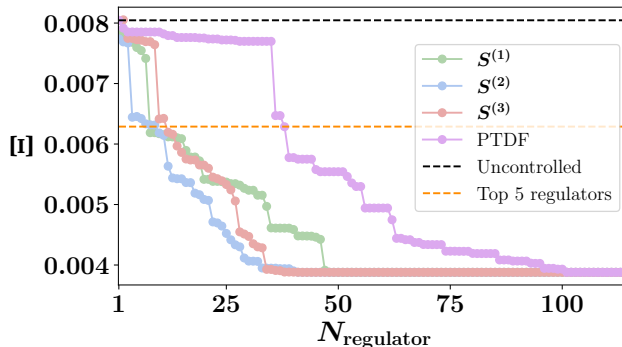


FIG. 3. Averaged frequency fluctuation Ξ vs. the number of regulators $N_{\text{regulator}}$ installed on the transmission lines in the UK power grid. The regulators are ordered by rank for each metric. $S^{(2)}$ achieves the best performance by only using less than one-third of all regulators. The orange dashed line is obtained from the AAC algorithm trained only with the top five ranked regulators in $S^{(2)}$.

algorithm to the original value, $|\hat{Y}_{ij} - Y_{ij}|$.

In Fig. 2(a)–(d), we mark the rank in color on each line for each measure, PTDF, $S^{(1)}$, $S^{(2)}$, and $S^{(3)}$, respectively. Lines with the top five ranks are marked with a star on their lines.

To evaluate the effectiveness of each ranking under the AAC algorithm, we employ average frequency fluctuations: $\Xi \equiv \frac{1}{L_f} \sum_{\ell} \Xi^{(\ell)}$, where L_f denotes the number of failure scenarios. We then measure Ξ while decreasing the number of admittance regulators $N_{\text{regulator}}$ for each metric. Fig. 3 illustrates Ξ for each measure as a function of $N_{\text{regulator}}$. We reach the minimum value of the fluctuations with ≈ 0.004 by installing regulators on only 35–45 top-rank

lines out of the total 114 possible lines. In particular, $S^{(2)}$ is found to be the best strategy, in which the minimum fluctuation level can be reached with 35 regulators and provides the lowest Ξ with fewer regulators.

Fig. 3 also shows that installing only five regulators in the order of $S^{(2)}$ significantly drops Ξ , indicating the existence of a sweet spot between cost and grid stability. Thus, we argue that installing five regulators with the highest ranks would efficiently reduce fluctuations and be cost-effective.

To verify the stabilization performance under the cost-effective regulators placement, we again train the AAC algorithm using only the top five regulators in $S^{(2)}$. As marked with an orange dashed line, the resulting performance is slightly better than that of the original model, which is trained with all regulators (except for the failure line) and then restricted to use only the five.

In short, the AAC algorithm is an integrated approach that effectively plans the line where the admittance regulator should be installed while simultaneously providing efficient operation.

III. CONNECTING TRANSIENT BEHAVIOR WITH THE STEADY STATE

We have shown that the AAC algorithm suppresses frequency fluctuations in the transient regime. Nevertheless, stability in the steady state is not guaranteed due to the nonlinearity of Eq. (1) and the heterogeneity of the power grid. To evaluate steady state stability, we examine the phase of each bus with and without the AAC intervention. The phase space is defined as a set of phases of each oscillator $\{\theta_1, \dots, \theta_N\}$. Suppose that the system is in steady state with $\{\theta_1^0, \dots, \theta_N^0\}$. A single line fault causes a dis-

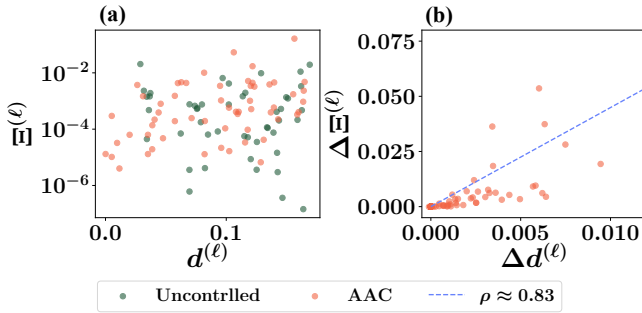


FIG. 4. Phase space analysis of the AAC algorithm’s operating mechanism. (a) Scatter plot showing the relationship between frequency fluctuations $\Xi^{(\ell)}$ and power flow variation $d^{(\ell)}$. The two quantities exhibit largely independent behavior. (b) The scatter plot shows the relationship between the reduction in frequency fluctuations $\Delta\Xi^{(\ell)}$ and the power flow restoration $\Delta d^{(\ell)}$. Each point corresponds to ℓ -th single-line failure in the UK grid.

turbance in the phase space, and then the system moves to another steady state $\{\theta_1^*, \dots, \theta_N^*\}$, where $\dot{\theta}_i^* = 0$ for all i .

In the steady state, we measure the fraction of power flow relative to the capacity of each line as follows:

$$I_{ij} \equiv |\sin(\theta_i - \theta_j)|. \quad (3)$$

Changes in steady state lead to large variations in I_{ij} , which may introduce instability to the system. Therefore, if the grid is optimally controlled in response to a disturbance, I_{ij} should return to its original value once steady state is recovered. We define the power flow variation $d^{(\ell)}$ in the phase space as

$$d^{(\ell)} = \frac{1}{L-1} \sum_{(i,j)} \left| I_{ij}^o - I_{ij}^{(\ell)} \right|, \quad (4)$$

where I_{ij}^o represents I_{ij} of line (i, j) in the original steady state and the superscript (ℓ) denotes the ℓ -th line failure scenario.

We first investigate the relationship between the transient regime frequency fluctuations $\Xi^{(\ell)}$ and the deviation of the power flow $d^{(\ell)}$ in the steady state. As shown in Fig. 4(a), these quantities exhibit negligible correlation over different ℓ regardless of the adjustment of the AAC algorithm. This reflects the weak dependency between the two regimes due to the inherent nonlinearity and heterogeneity of the system.

In contrast, Fig. 4(b) presents a markedly different result when examining control-induced changes. We first observe that $d^{(\ell)}$ decreases after AAC intervention for all ℓ , corresponding to an increase in the power-flow restoration measure $\Delta d^{(\ell)}$, demonstrating that AAC stabilizes both transient dynamics and steady state conditions. Furthermore, the Pearson correlation coefficient ρ between the decrease in frequency fluctuation $\Delta\Xi^{(\ell)}$ and the restoration of power flow $\Delta d^{(\ell)}$ is close to one ($\rho \approx 0.83$), indicating that the AAC algorithm effectively relates the two regimes.

IV. DISCUSSION

We illustrate that artificial intelligence (AI) is capable of effectively stabilizing the power grid by strategically and adaptively controlling transmission line admittances in response to single-line fault events, which is the most common type of disturbance. The proposed Adaptive Admittance Controller (AAC) algorithm integrates the typically distinct layers of grid planning and real-time operation into a single reinforcement learning framework. Addresses a few key issues faced by grid operators transitioning to renewable grids. Firstly, it demonstrates selective intervention, achieving an average 53% reduction in frequency fluctuations, while avoiding unnecessary interventions during negligible disturbances (Fig. 1). Secondly, strategic placement of regulators on five critical transmission lines results in near-optimal stabilization while cutting implementation costs by more than 95% compared to comprehensive deployment. These combined capabilities directly address the main challenges of transitioning to renewable energy—namely reduced system inertia and increased operational complexity. The ranking method derived from the AAC algorithm has been proven to be most effective in identifying these critical locations, outperforming traditional PTDF-based approaches (Figs. 2 and 3).

The algorithm showcases impressive economic efficiency, addressing a major hurdle in smart grid deployment: the exorbitant cost of large-scale FACTS installations, each priced at \$ 20 million and necessitating years of regulatory approval [41, 42]. In addition to its economic advantages, the AAC algorithm exhibits a notable capability: simultaneously stabilizing both the transient regime and the steady state regime. Although frequency fluctuations and power flow deviations appear independent at first glance, their reductions under the AAC intervention are strongly correlated, as shown in Fig. 4. This indicates that the AAC algorithm successfully overcomes a challenge posed by system nonlinearity which typically obscures the relationship between these regimes.

Based on these findings, the basic feasibility of AI-driven transmission control presents various promising avenues for further investigation. Firstly, while a simplified version of the UK power grid is used due to high computational demands, applying the AAC algorithm to functional grids in the field remains crucial for broad implementation. Secondly, extending the framework to accommodate multiple concurrent faults would assess its resilience under more challenging operating conditions. Lastly, integrating the renewable energy forecasting service would allow the system to respond proactively to potential instabilities. This study could serve as the foundation for future self-optimizing grids, where intelligent algorithms autonomously maintain stability even amid

the growing complexity driven by renewable energy.

As power grids experience their most significant change in 100 years, AI offers a viable route to ensure stability. Beyond power grids, this work suggests broader potential applications within network science to suppress cascading failures through adaptive link weight control. The failure mechanism we address—where a single disruption triggers flow redistribution that overloads other links—appears across critical infrastructures, including road closures causing congestion cascades, fuse failures triggering electrical outages, and node failures redirecting data flow. The core insight of the AAC framework—that controlling a small number of critical links can prevent system-wide cascades—may provide a general template for domains in which nonlinear dynamics render analytical prediction intractable. Our findings indicate that intelligent, adaptive control is essential for reliable power grid operation and could prove valuable for other complex networked systems.

V. METHODS

We formulate the stability control problem as an RL task in which an agent learns to adjust transmission line admittances after faults. The task requires making two interdependent choices: which lines to control and to what extent. This results in a high-dimensional search space, which increases exponentially with the number of regulators.

Single-step episode. A standard RL setting expects a sequential Markov Decision Process where the agent takes multiple actions in response to the environment. However, in practical grid operations, repeated interventions increase operational cost. To reflect this, we adopt a single-step episode design in which the agent takes action only once per fault event. Fig. 5 illustrates the general framework of the AAC algorithm and its interaction with the environment: the power grid.

Positioning of the regulator. The regulators are assumed to be located on all transmission lines. Exceptionally, to obtain Fig. 3, some regulators are removed based on their ranking. Note that the AAC result for the top 5 regulators is trained from scratch under these conditions.

State representation. The state of the system is provided as input to the agent. Formally, the state is represented as $X \equiv \{\mathbf{m}, \boldsymbol{\gamma}, \mathbf{P}, \boldsymbol{\theta}, \dot{\boldsymbol{\theta}}, \mathbf{b}, \mathbf{Y}\}$, where $\mathbf{m} \equiv \{m_1, \dots, m_N\}$, $\boldsymbol{\gamma} \equiv \{\gamma_1, \dots, \gamma_N\}$, $\mathbf{P} \equiv \{P_1, \dots, P_N\}$, $\boldsymbol{\theta} \equiv \{\cos \theta_1, \sin \theta_1, \dots, \cos \theta_N, \sin \theta_N\}$, and $\dot{\boldsymbol{\theta}} \equiv \{\dot{\theta}_1, \dots, \dot{\theta}_N\}$. $\mathbf{b} \equiv \{b_1, \dots, b_N\}$ is a binary value that indicates whether the bus is connected to the fault line, and \mathbf{Y} is the admittance matrix of the modified transmission lines so that $Y_{uv} = Y_{vu} = 0$ for the fault line $\ell = (u, v)$.

Policy network and action space. To capture long-range interactions, we employ the Chebyshev convolution [43], a branch of GNN. It incorporates features from

distant nodes to update the target node's feature. Based on observation X , the node features are transformed into high-dimensional features through the convolution layers. For each transmission line (i, j) , the characteristic of the line is constructed by concatenating the node features of i and j . The policy network then produces two outputs for the regulator line through separate layers: $C_{ij} \in [0, 1]$ from the control layer, and μ_{ij} and σ_{ij} from the adjustment layer. From C_{ij} , binary control decision $c_{ij} \sim \pi_c = \text{Bernoulli}(C_{ij})$ is sampled during training and $c_{ij} = C_{ij}$ during evaluation. Similarly, from μ_{ij} and σ_{ij} , adjustment magnitude $q_{ij} \sim \pi_q = \mathcal{N}(\mu_{ij}, \sigma_{ij})$ is sampled during training and $q_{ij} = \mu_{ij}$ during evaluation. c_{ij} and q_{ij} are combined with $\chi_{ij} \in \{0, 1\}$, which indicates whether the line (i, j) is equipped with a regulator. Finally, the adjusted admittance $\hat{\mathbf{Y}}$ is obtained as

$$\hat{Y}_{ij} = 2^{\delta y_{ij}} Y_{ij}, \quad \text{where } \delta y_{ij} = c_{ij} q_{ij} \chi_{ij}. \quad (5)$$

This formulation allows for both increases ($\delta y_{ij} > 0$) and decreases ($\delta y_{ij} < 0$) in admittance, with $\hat{Y}_{ij} = Y_{ij}$ when $c_{ij} = 0$

Reward design. The environment evaluates the updated state and computes a reward $R^{(\ell)}$ to guide policy learning. The reward balances stability improvement against control complexity:

$$R^{(\ell)} = \begin{cases} \frac{\Delta \Xi^{(\ell)}}{1 + 0.05 \sum_{(i,j)} c_{ij}} & \text{if } \Delta \Xi^{(\ell)} \neq 0, \\ R_c & \text{otherwise.} \end{cases}$$

To compute the decrease in frequency fluctuation $\Delta \Xi^{(\ell)}$, we set $T = 2$ seconds for rapid policy updates during training, while $T = 10$ seconds is used in evaluation to complete the evaluation of long-term stability. The denominator of $R^{(\ell)}$ penalizes excessive use of regulators, and the coefficient 0.05 is empirically chosen as the value that yielded the most stable training performance. The constant R_c provides a small positive reward to discourage unnecessary interventions when control has no effect. During training, we chose $R_c = 10^{-5}$ for the UK power grid, as this value produced the best performance.

Policy optimization. As discussed above, the AAC algorithm has two decision distributions: π_c for c_{ij} and π_q for q_{ij} . The joint probability distribution can be written as

$$\log \pi(\mathbf{c}, \mathbf{q}|X) = \log \pi_c(\mathbf{c}|X) + \mathbf{c} \log \pi_q(\mathbf{q}|X), \quad (6)$$

where \mathbf{c} acts as a mask for π_q , ensuring that the adjustment distribution contributes only when the control is applied.

To find the optimal policy $\pi(\mathbf{c}, \mathbf{q}|X)$ that maximizes reward $R^{(\ell)}$, we employ Proximal Policy Optimization (PPO) [44]. The standard PPO uses a value network to estimate a baseline for calculating the advantage. However, value network often requires sufficient training and

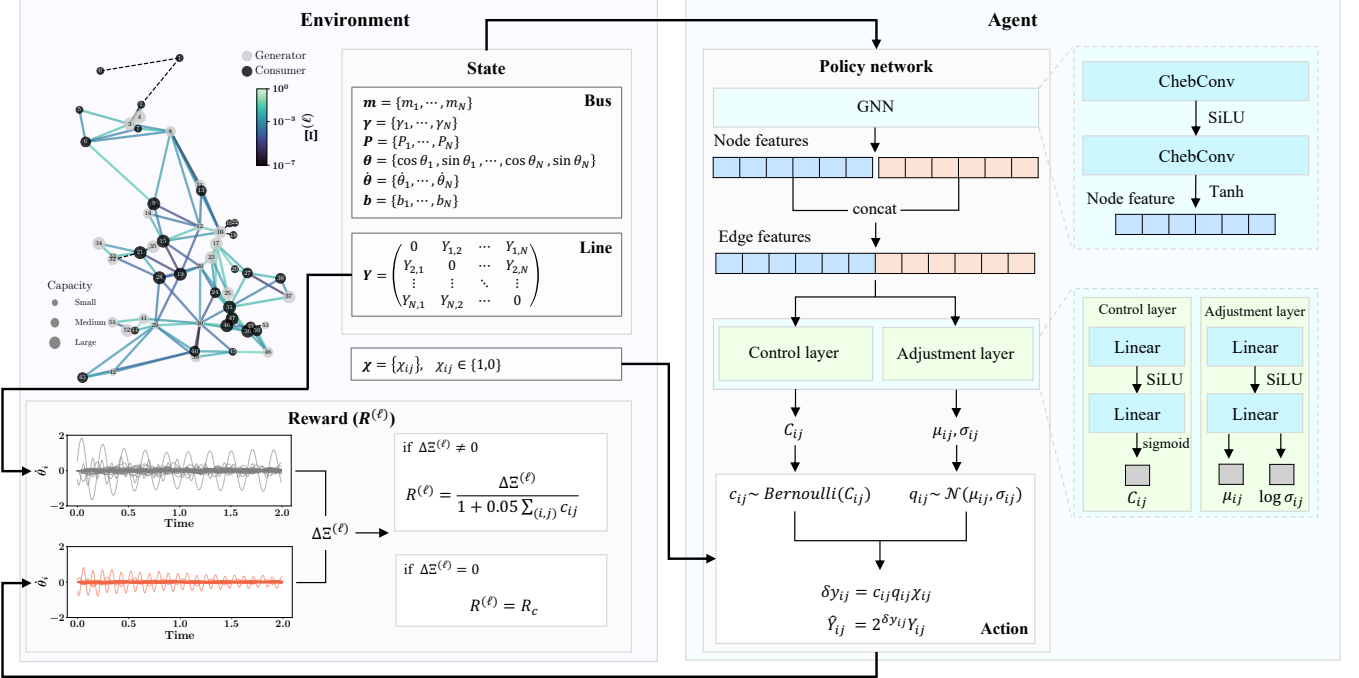


FIG. 5. Reinforcement learning framework for the AAC algorithm. The agent observes the power grid state, including system parameters and failed transmission line ℓ . Based on this observation, it outputs two control signals for each non-failed line: C_{ij} from control layer and μ_{ij}, σ_{ij} from adjustment layer. A binary decision $c_{ij} \sim \text{Bernoulli}(C_{ij})$ indicating whether to apply control, and a continuous adjustment magnitude $q_{ij} \sim \mathcal{N}(\mu_{ij}, \sigma_{ij})$. These are combined with regulator presence vector χ_{ij} into the final action δy_{ij} . The admittances in power grid are then updated to \hat{Y}_{ij} and a reward $R^{(\ell)}$ is evaluated, which reflects both frequency stability and control efficiency. The AAC is trained to maximize the averaged reward over all possible ℓ by iterating this loop.

may yield inaccurate advantages when underfitting [45]. Several previous studies, therefore, omit them in similar contexts [46–48].

In our single-step setting, the reward is immediate, so

the value network is not required. Accordingly, the loss function of the AAC algorithm utilizing PPO is defined as

$$\mathcal{L}^{(\ell)} = -\max \left[\frac{\pi(\mathbf{c}, \mathbf{q}|X)}{\pi^{\text{old}}(\mathbf{c}, \mathbf{q}|X)} R^{(\ell)}, \text{clip} \left(\frac{\pi(\mathbf{c}, \mathbf{q}|X)}{\pi^{\text{old}}(\mathbf{c}, \mathbf{q}|X)}, 1 - \epsilon, 1 + \epsilon \right) R^{(\ell)} \right], \quad (7)$$

where $\pi^{\text{old}}(\mathbf{c}, \mathbf{q}|X)$ denotes previous joint policy, and $\epsilon = 0.1$ is chosen for the clipping parameter.

$\mathcal{L}^{(\ell)}$ is averaged on all ℓ -th single-line failures, and the policy network is updated through gradient ascent to maximize expected reward.

During the preparation of this work, the author(s) used Claude Sonnet 4.5 and ChatGPT 5.2 to improve the clarity and readability of the language. After using these tool/service, the author(s) reviewed and edited the content as needed and take(s) full responsibility for the content of the publication.

ACKNOWLEDGMENTS

This work was supported by the Korea Institute of Energy Technology Evaluation and Planning(KETEP) and the Ministry of Trade, Industry & Energy(MOTIE) of the Republic of Korea (No. 20224000000100) (BK), and the National Research Foundation of Korea (NRF) grant funded by the Korea Government (MSIT) (No. RS-2025-00556024) (HY).

[1] B. Obama, Presidential policy directive 21–critical infrastructure security and resilience (2013).

[2] S. M. Rinaldi, J. P. Peerenboom, and T. K. Kelly, Identifi-

fying, understanding, and analyzing critical infrastructure interdependencies, *IEEE control systems magazine* **21**, 11 (2001).

[3] N. Shaukat, S. Ali, C. Mehmood, B. Khan, M. Jawad, U. Farid, Z. Ullah, S. Anwar, and M. Majid, A survey on consumers empowerment, communication technologies, and renewable generation penetration within smart grid, *Renewable and Sustainable Energy Reviews* **81**, 1453 (2018).

[4] A. Gulraiz, S. Sajjad Haider Zaidi, and B. Mohammad Khan, Advancing energy integration: renewable sources, ancillary services, and stability, *PloS one* **20**, e0324812 (2025).

[5] A. Crivellaro, A. Tayyebi, C. Gavriluta, D. Groß, A. Anta, F. Kupzog, and F. Dörfler, Beyond low-inertia systems: Massive integration of grid-forming power converters in transmission grids, in *2020 IEEE power & energy society general meeting (PESGM)* (IEEE, 2020) pp. 1–5.

[6] M. Khalid, Smart grids and renewable energy systems: Perspectives and grid integration challenges, *Energy Strategy Reviews* **51**, 101299 (2024).

[7] K. Y. Yap, C. R. Sarimuthu, and J. M.-Y. Lim, Virtual inertia-based inverters for mitigating frequency instability in grid-connected renewable energy system: A review, *Applied Sciences* **9**, 5300 (2019).

[8] T. Kerdphol, F. S. Rahman, and Y. Mitani, Virtual inertia control application to enhance frequency stability of interconnected power systems with high renewable energy penetration, *Energies* **11**, 981 (2018).

[9] O. Smith, O. Cattell, E. Farcot, R. D. O’Dea, and K. I. Hopcraft, The effect of renewable energy incorporation on power grid stability and resilience, *Science advances* **8**, eabj6734 (2022).

[10] J. Bialek, What does the gb power outage on 9 august 2019 tell us about the current state of decarbonised power systems?, *Energy Policy* **146**, 111821 (2020).

[11] G. Zhang, H. Zhong, Z. Tan, T. Cheng, Q. Xia, and C. Kang, Texas electric power crisis of 2021 warns of a new blackout mechanism, *CSEE journal of Power and Energy Systems* **8**, 1 (2022).

[12] N. M. Flores, H. McBrien, V. Do, M. V. Kiang, J. Schlegelmilch, and J. A. Casey, The 2021 texas power crisis: distribution, duration, and disparities, *Journal of exposure science & environmental epidemiology* **33**, 21 (2023).

[13] N. Sharma, A. Acharya, I. Jacob, S. Yamujala, V. Gupta, and R. Bhakar, Major blackouts of the decade: Underlying causes, recommendations and arising challenges, in *2021 9th IEEE International Conference on Power Systems (ICPS)* (IEEE, 2021) pp. 1–6.

[14] M. A. Raza, K. L. Khatri, A. Hussain, M. H. A. Khan, A. Shah, and H. Taj, Analysis and proposed remedies for power system blackouts around the globe, *Engineering Proceedings* **20**, 5 (2022).

[15] J. Stürmer, A. Plietzsch, T. Vogt, F. Hellmann, J. Kurths, C. Otto, K. Frieler, and M. Anvari, Increasing the resilience of the texas power grid against extreme storms by hardening critical lines, *Nature Energy* **9**, 526 (2024).

[16] L. Pagnier and P. Jacquod, Inertia location and slow network modes determine disturbance propagation in large-scale power grids, *PloS one* **14**, e0213550 (2019).

[17] A. Fernández-Guillamón, E. Muljadi, and A. Molina-García, Frequency control studies: A review of power system, conventional and renewable generation unit model- ing, *Electric Power Systems Research* **211**, 108191 (2022).

[18] B. Schäfer, D. Witthaut, M. Timme, and V. Latora, Dynamically induced cascading failures in power grids, *Nature communications* **9**, 1975 (2018).

[19] S. Pahwa, C. Scoglio, and A. Scala, Abruptness of cascade failures in power grids, *Scientific reports* **4**, 3694 (2014).

[20] Y. Zhang and O. Yağan, Optimizing the robustness of electrical power systems against cascading failures, *Scientific reports* **6**, 27625 (2016).

[21] Y. Dai, R. Preece, and M. Panteli, Risk assessment of cascading failures in power systems with increasing wind penetration, *Electric Power Systems Research* **211**, 108392 (2022).

[22] J. Alexander, Oscillatory solutions of a model system of nonlinear swing equations, *International Journal of Electrical Power & Energy Systems* **8**, 130 (1986).

[23] Q. Qiu, R. Ma, J. Kurths, and M. Zhan, Swing equation in power systems: Approximate analytical solution and bifurcation curve estimate, *Chaos: An Interdisciplinary Journal of Nonlinear Science* **30** (2020).

[24] G. Ódor, I. Papp, K. Benedek, and B. Hartmann, Improving power-grid systems via topological changes or how self-organized criticality can help power grids, *Physical Review Research* **6**, 013194 (2024).

[25] B. Schäfer, T. Pesch, D. Manik, J. Gollenstede, G. Lin, H.-P. Beck, D. Witthaut, and M. Timme, Understanding braess’ paradox in power grids, *Nature Communications* **13**, 5396 (2022).

[26] N. L. Cain and H. T. Nelson, What drives opposition to high-voltage transmission lines?, *Land use policy* **33**, 204 (2013).

[27] J. Cohen, K. Moeltner, J. Reichl, and M. Schmidthaler, An empirical analysis of local opposition to new transmission lines across the eu-27, *The Energy Journal* **37**, 59 (2016).

[28] H.-J. Lee, S.-H. Kim, K. Hur, J.-S. Choi, H.-J. Oh, B.-J. Lee, G. Jang, and J. H. Chow, Integrating tcsc to enhance transmission capability and security: Feasibility studies for korean electric power system, in *2016 IEEE Power and Energy Society General Meeting (PESGM)* (IEEE, 2016) pp. 1–6.

[29] Z. Azimi and G. Shahgholian, Power system transient stability enhancement with tcsc controller using genetic algorithm optimization, *International Journal of Natural and Engineering Sciences* **10**, 09–15 (2019).

[30] I. E. Nkan, E. E. Okpo, and A. B. Inyang, Enhancement of power systems transient stability with tcsc: a case study of the nigerian 330 kv, 48-bus network, *International Journal of Multidisciplinary Research and Analysis* **6**, 4828 (2023).

[31] D. Silver, A. Huang, C. J. Maddison, A. Guez, L. Sifre, G. Van Den Driessche, J. Schrittwieser, I. Antonoglou, V. Panneershelvam, M. Lanctot, *et al.*, Mastering the game of go with deep neural networks and tree search, *nature* **529**, 484 (2016).

[32] A. Mirhoseini, A. Goldie, M. Yazgan, J. W. Jiang, E. Songhori, S. Wang, Y.-J. Lee, E. Johnson, O. Pathak, A. Nova, *et al.*, A graph placement methodology for fast chip design, *Nature* **594**, 207 (2021).

[33] J. Degrave, F. Felici, J. Buchli, M. Neunert, B. Tracey, F. Carpanese, T. Ewalds, R. Hafner, A. Abdolmaleki, D. de Las Casas, *et al.*, Magnetic control of tokamak plasmas through deep reinforcement learning, *Nature* **602**, 414 (2022).

[34] S. Jo, J.-Y. Oh, Y. T. Yoon, and Y. G. Jin, Self-healing

radial distribution network reconfiguration based on deep reinforcement learning, *Results in Engineering* **22**, 102026 (2024).

[35] R. A. Jacob, S. Paul, S. Chowdhury, Y. R. Gel, and J. Zhang, Real-time outage management in active distribution networks using reinforcement learning over graphs, *Nature Communications* **15**, 4766 (2024).

[36] Y. Lee, H. Choi, L. Pagnier, C. H. Kim, J. Lee, B. Jhun, H. Kim, J. Kurths, and B. Kahng, Reinforcement learning optimizes power dispatch in decentralized power grid, *Chaos, Solitons & Fractals* **186**, 115293 (2024).

[37] R. Huang, W. Gao, R. Fan, and Q. Huang, Damping inter-area oscillation using reinforcement learning controlled tcsc, *IET Generation, Transmission & Distribution* **16**, 2265 (2022).

[38] D. Ernst, M. Glavic, and L. Wehenkel, Power systems stability control: reinforcement learning framework, *IEEE transactions on power systems* **19**, 427 (2004).

[39] P. Schultz, J. Heitzig, and J. Kurths, A random growth model for power grids and other spatially embedded infrastructure networks, *The European Physical Journal Special Topics* **223**, 2593 (2014).

[40] A. J. Wood, B. F. Wollenberg, and G. B. Sheblé, *Power generation, operation, and control* (John Wiley & Sons, 2013).

[41] K. Habur and D. O’Leary, Facts-flexible alternating current transmission systems: for cost effective and reliable transmission of electrical energy, Siemens-World Bank document-Final Draft Report, Erlangen **46**, 244 (2004).

[42] G. Longoria, M. Lynch, N. Farrell, and J. A. Curtis, *The impact of planning and regulatory delays for major energy infrastructure*, Tech. Rep. (ESRI Working Paper, 2022).

[43] M. Defferrard, X. Bresson, and P. Vandergheynst, Convolutional neural networks on graphs with fast localized spectral filtering, *Advances in neural information processing systems* **29** (2016).

[44] J. Schulman, F. Wolski, P. Dhariwal, A. Radford, and O. Klimov, Proximal policy optimization algorithms, arXiv preprint arXiv:1707.06347 (2017).

[45] S. Moalla, A. Miele, D. Pyatko, R. Pascanu, and C. Gulcehre, No representation, no trust: connecting representation, collapse, and trust issues in ppo, *Advances in Neural Information Processing Systems* **37**, 69652 (2024).

[46] Z. Shao, P. Wang, Q. Zhu, R. Xu, J. Song, X. Bi, H. Zhang, M. Zhang, Y. Li, Y. Wu, *et al.*, Deepseekmath: Pushing the limits of mathematical reasoning in open language models, arXiv preprint arXiv:2402.03300 (2024).

[47] R. Rafailov, A. Sharma, E. Mitchell, C. D. Manning, S. Ermon, and C. Finn, Direct preference optimization: Your language model is secretly a reward model, *Advances in neural information processing systems* **36**, 53728 (2023).

[48] Q. Zhang and L. Ying, Zeroth-order policy gradient for reinforcement learning from human feedback without reward inference, arXiv preprint arXiv:2409.17401 (2024).

SUPPLEMENTARY INFORMATION

A. Topological and Dynamical Characteristics of the SHK Network

To verify that the performance of the AAC algorithm is not confined to heterogeneous real-world grids, we tested it on an SHK network with more homogeneous parameters. The SHK network is a synthetic model commonly used to investigate the dynamics of the power grid. Its topology is determined by four parameters p , q , r , and s . In this study, we generate the SHK network whose properties closely match those of the reduced UK power grid. To identify suitable parameters, we compare several topological metrics with those of the UK grid [Fig. 1(a)]: the second-smallest eigenvalue of the Laplacian matrix λ , mean degree \bar{k} , mean clustering coefficient (cc), diameter, and average length of the shortest path (aspl). We find that $p = 0.4$, $q = 0.9$, $r = 0.1$, and $s = 0.2$ agrees closely across all metrics. Supplementary Table 1 shows that the resulting SHK network matches the UK grid not only in network size N and number of links L , but also in its key topological characteristics.

	N	L	\bar{k}	λ	cc	diameter	aspl
UK	54	114	4.222	0.1212	0.5025	10	3.712
SHK	54	115	4.259	0.1187	0.4070	8	3.703

TABLE I. Topological properties of UK power grid and the SHK network ($p = 0.4$, $q = 0.9$, $r = 0.1$, $s = 0.2$).

In the SHK network, generators and consumers are randomly assigned [Fig. 6]. To study a relatively homogeneous power grid, we set most of the parameters of the swing equation [Eq. (1)] to uniform values: generator and consumer powers are assigned as $+1$ or -1 , respectively; inertia constants m_i and damping coefficients γ_i are set to the average values observed in the UK power grid; and all coupling strengths are fixed at $K_{ij} = 4$. As shown in Fig. 6, even with reduced parameter heterogeneity, the frequency fluctuations $\Xi^{(\ell)}$ over 10 seconds still depend on the location of the fault line ℓ . Therefore, in a relatively homogeneous grid, effective regulator locations must still be tailored to each specific fault scenario.

B. AAC algorithm Performance in the SHK Network

In the main text, we showed that the adaptive admittance controller (AAC) algorithm can effectively decrease $\Xi^{(\ell)}$ in the UK power grid, which exhibits heterogeneity in the parameters of the swing equation [Eq. (1)]. Here, we analyze its performance in the SHK network, which has more homogeneous characteristics than the UK grid. To ensure effective performance, it is necessary to choose an appropriate R_c , as this parameter influences the control tendencies of the AAC algorithm. We find that $R_c = 10^{-5}$

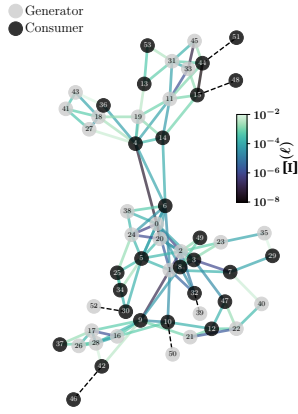


FIG. 6. The frequency fluctuations $\Xi^{(\ell)}$ in the generated SHK network ($p = 0.4$, $q = 0.9$, $r = 0.1$, $s = 0.2$). Black dashed lines indicate fault scenarios that are excluded from the analysis, as disconnecting these lines would split the power grid into two isolated parts.

produces appropriate behavior. As shown in Fig. 7, the AAC algorithm reduces $\Xi^{(\ell)}$ in high-impact fault scenarios while maintaining $\Xi^{(\ell)}$ in low-impact scenarios by avoiding unnecessary interventions. The AAC algorithm achieves an approximately 55% reduction in the average frequency fluctuation in the SHK network. This shows that the AAC algorithm can effectively suppress $\Xi^{(\ell)}$ even in a homogeneous power grid.

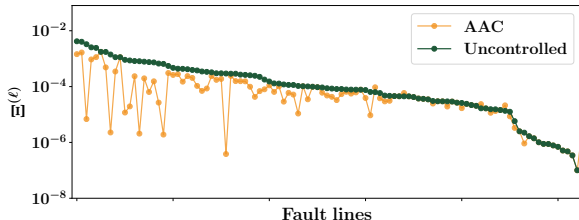


FIG. 7. The frequency fluctuations $\Xi^{(\ell)}$ for the non-control case (green) and the AAC algorithm case (orange) across all single-line failures in the SHK network. Fault scenarios are sorted by the magnitude of $\Xi^{(\ell)}$ in the uncontrolled case. AAC algorithm results show that $\Xi^{(\ell)}$ is significantly reduced in high- $\Xi^{(\ell)}$ scenarios, while in low- $\Xi^{(\ell)}$ cases the algorithm tends to avoid intervention.

The AAC algorithm adjusts Y_{ij} differently depending on the fault scenario, resulting in certain locations being

frequently modified [Fig. 2]. A similar pattern is observed in the SHK network. Fig. 8 shows the average Ξ across all fault scenarios as a function of the number of regulators $N_{\text{regulator}}$ used. Unlike in the UK power grid, we omit PTDF-based measurements due to the absence of a slack bus, and $S^{(3)}$ because all $K_{ij} = 4$ in the SHK network, making $S^{(3)}$ equivalent to $S^{(2)}$ up to a constant factor.

As shown in Fig. 8, the minimum fluctuation level can be achieved without installing regulators on all transmission lines. In particular, $S^{(2)}$ reaches the minimum Ξ with only 74 regulators out of 115 possible lines, demonstrating that strategic placement on a subset of lines is sufficient for optimal performance. $S^{(2)}$ achieves the best performance compared to $S^{(1)}$, confirming that $S^{(2)}$ is the most effective ranking metric for both the SHK network and the UK grid.

Although the AAC algorithm effectively suppresses frequency fluctuations in the transient regime [Fig. 7], the steady state stability is not guaranteed due to the system's nonlinearity. To evaluate this, we examine the power flow variation $d^{(\ell)}$ in phase space, as defined in Eq. (4).

As shown in Fig. 9(a), $\Xi^{(\ell)}$ and $d^{(\ell)}$ exhibit negligible correlation, indicating that transient regime frequency fluctuations and power flow deviations in the steady state are largely independent due to nonlinearity. In contrast, Fig. 9(b) reveals that control-induced changes are strongly correlated. The Pearson correlation coefficient ρ between $\Delta\Xi^{(\ell)}$ and $\Delta d^{(\ell)}$ is approximately 0.81, demonstrating that the AAC algorithm effectively bridges the nonlinearity-induced gap between the two regimes. These results confirm that the AAC algorithm simultaneously stabilizes both transient dynamics and steady state in the SHK network.

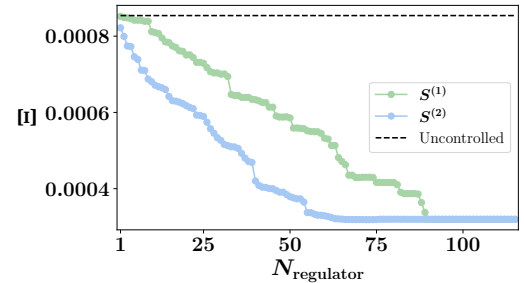


FIG. 8. Averaged frequency fluctuation Ξ vs. the number of regulators $N_{\text{regulator}}$ installed on the transmission lines in the SHK network. The regulators are ordered by rank for each metric. $S^{(2)}$ achieves the best performance by only using less than one-half of all regulators.

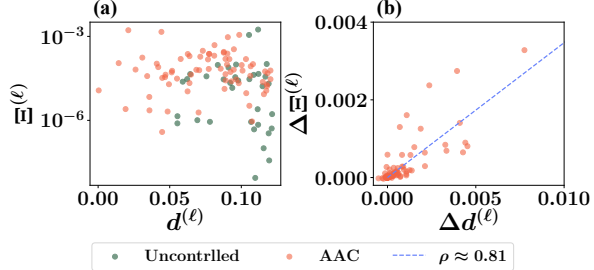


FIG. 9. Phase space analysis of the AAC algorithm's operating mechanism in the SHK network. (a) Scatter plot showing the relationship between frequency fluctuations $\Xi^{(\ell)}$ and power flow variation $d^{(\ell)}$. The two quantities exhibit largely independent behavior. (b) The scatter plot shows the relationship between the reduction in frequency fluctuations $\Delta\Xi^{(\ell)}$ and power flow restoration $\Delta d^{(\ell)}$. Each point corresponds to ℓ -th single-line failure in the SHK network.